J. G. Pinto, Vítor Monteiro, Henrique Gonçalves, João L. Afonso

"OnBoard Reconfigurable Battery Charger for Electric Vehicles with Traction-to-Auxiliary Mode"

IEEE Transactions on Vehicular Technology, vol.63, no.3, pp.1104-1116, Mar. 2014.

http://ieeexplore.ieee.org/stamp/stamp.jsp?arnumber=6609093

ISSN: 0018-9545

DOI: 10.1109/TVT.2013.2283531

J. G. Pinto, Vítor Monteiro, Henrique Gonçalves, João L. Afonso, "OnBoard Reconfigurable Battery Charger for Electric Vehicles with Traction-to-Auxiliary Mode," IEEE Transactions on Vehicular Technology, vol.63, no.3, pp.1104-1116, Mar. 2014. ISSN 0018-9545, DOI: 10.1109/TVT.2013.2283531

On-Board Reconfigurable Battery Charger for Electric Vehicles with Traction-to-Auxiliary Mode

J. G. Pinto, *Student Member, IEEE,* Vítor Monteiro, *Student Member, IEEE,*
Henrique Gonçalves, *Member, IEEE,* João L. Afonso, *Member, IEEE*

***Abstract*—This paper proposes a single-phase reconfigurable battery charger for Electric Vehicle (EV) that operates in three different modes: Grid-to-Vehicle (G2V) mode, in which the traction batteries are charged from the power grid; Vehicle-to-Grid (V2G) mode, in which the traction batteries deliver part of the stored energy back to the power grid; and in Traction-to-Auxiliary (T2A) mode, in which the auxiliary battery is charged from the traction batteries. When connected to the power grid, the battery charger works with sinusoidal current in the AC side, for both G2V and V2G modes, and also regulates the reactive power. When the EV is disconnected from the power grid, the control algorithms are modified and the full-bridge AC-DC bidirectional converter works as a full-bridge isolated DC-DC converter that is used to charge the auxiliary battery of the EV, avoiding the use of an additional charger to accomplish this task. To assess the behavior of the proposed reconfigurable battery charger under different operation scenarios, a 3.6 kW laboratory prototype has been developed and experimental results are presented.**

***Index Terms*—Battery Charger, Electric Vehicles, Grid-to-Vehicle (G2V), Power Quality, Traction-to-Auxiliary (T2A), Vehicle to Grid (V2G)**

I. Introduction

THE interest on technologies for Electric Vehicles (EVs) and Plug-in Hybrid Electric Vehicles (PHEVs) has significantly increased in the last years, as reflected in the number of scientific publications [1]-[4]. Besides the increasing interest on the subject, it is predictable that the number of EVs will immensely grow in the next decades. In a baseline forecast electric cars will account for 64% of U.S. light-vehicle sales by 2030 and will comprise 24% of the U.S. light-vehicle fleet by this year [5]. However, the power grids were not designed for this new type of load, and therefore the impact caused by the proliferation of EVs cannot be neglected [6], [7]. Nevertheless, EVs have the capability to store a significant amount of energy in their traction batteries (the batteries used to store the energy that is provided to the powertrain of the EV), and if a large number of EVs operate in a coordinate way using bidirectional battery chargers, they can be used to balance the production and consumption of energy of the electrical power grid [8]. One factor that supports that such collaboration between EVs and electrical power grids may exist relates to the fact that private vehicles are parked on average 93-96% of their lifetime, such that, during that time each vehicle represents an idle asset [9]. Using adequate power converters and control algorithms, the battery chargers of EVs can regulate both the active and the reactive power flow from the power grid, contributing to stabilize the electrical system voltage and frequency [10]-[12]. The integration of EVs in the power grids will be a fundamental part in the future Smart Grids. The denominated Vehicle-to-Grid (V2G) paradigm, in which the traction batteries of the EVs deliver part of the stored energy back to the power grid, is expected to be one of the key technologies in the future of the Smart Grids [13], [14]. With a simpler way to access the energy market it is predictable that EV users will intend to participate in the energy market, according to their convenience, profiting from the energy price variations along the day in order to have a payback from the V2G operation mode. From 2015 to 2020, it is expected that the global V2G vehicle unit sales will grow from about 100 thousands to more than 1 million, which means an annual growth rate from 2015 to 2020 of 59% [15]. Therefore, the development of solutions that allow the integration of EVs in Smart Grids is a subject of utmost importance. Aware of this, many researchers have focused their scientific investigations in the design and implementation of optimized topologies towards on-board battery chargers [16]-[18].

Nowadays, two main EVs charging solutions are being researched: the inductive and the conductive methods. In the conductive method there is an electrical contact between the vehicle and the power grid, and in the inductive method there is no electrical contact between the vehicle and the power grid [19]. Although the recent progresses in the inductive method [20], [21], the most common solutions are based on the

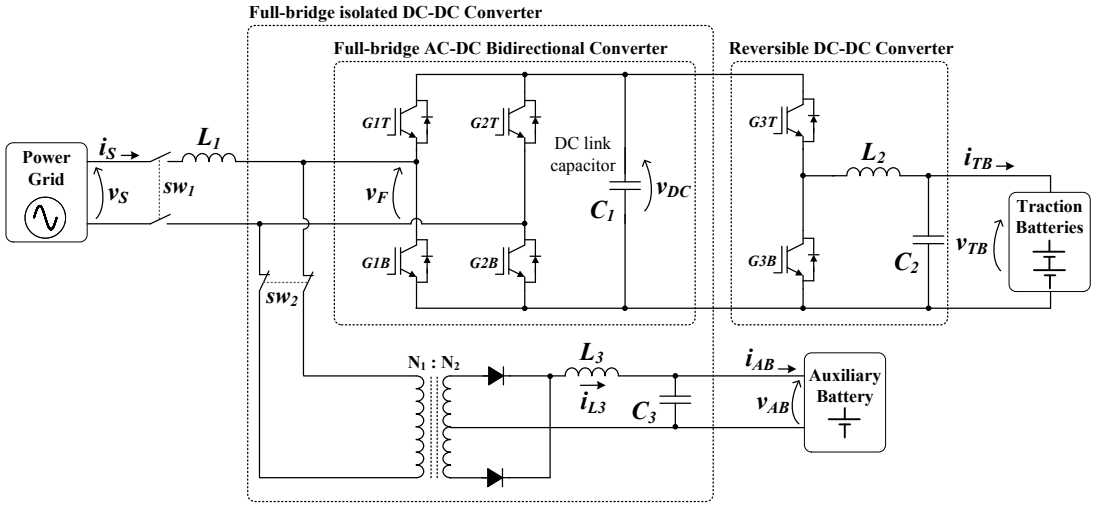

Fig. 1. Reconfigurable battery charger composed by three power stages: Full-bridge AC-DC bidirectional converter; Reversible DC-DC converter; Full-bridge isolated DC-DC converter.

conductive method [22]. The majority of EVs are being designed with conductive method on-board unidirectional battery chargers specified by IEC 61851-1 standard, Mode 1, 2, and 3 [23]. These unidirectional battery chargers only permit operation in Grid-to-Vehicle (G2V) mode, in which the traction batteries are charged from the power grid. In addition to the on-board battery chargers, some vehicles allow the possibility of charging their batteries with off-board unidirectional chargers, specified by IEC 61851-1 standard Mode 4.

Various solutions for battery chargers of EVs operating in G2V mode have been proposed in recent years. In [24] is proposed a battery charger for PHEVs based on the buck converter with controllable power factor. This topology is composed by a single-stage H-bridge aiming to reduce the size and weight of the charger. Besides the conventional bridge boost PFC (Power Factor Correction) topologies [16], [25], in [26] is presented an overview of the bridgeless boost PFC topologies. In [27] is presented an innovative topology based on a three-phase ultra-sparse matrix converter, that absorbs currents with low total harmonic distortion and nearly unitary power factor over a wide output power range, from zero to full load.

Aiming to accomplish with V2G mode of operation it is necessary to use battery chargers with bidirectional power converter topologies, reviewed in [28] and [29]. A five-level bidirectional grid interface with a DC-DC converter to provide a regulated DC link voltage to the motor drive and to capture the braking energy during regenerative braking is presented in [30]. More recently, multi-functional modes of operation are being proposed. In [31] is proposed a bidirectional battery charger for PHEVs that can operate in the G2V, V2G and Vehicle-to-Home (V2H) modes. Although all of these research works present interesting functionalities, none of them proposes an important functionality, which consists in charging the vehicle auxiliary battery (the 12 V battery that feeds lighting and signaling circuits, windshield wiper, stereo sound system, GPS and all of the others cockpit functionalities). In Internal Combustion Engines (ICE) vehicles, the auxiliary battery is usually charged from an electric generator (alternator) coupled to the traction motor. In EVs and PHEVs the alternator is replaced by an extra DC-DC converter that charges the auxiliary battery from the traction batteries.

In [32] is proposed a multi-functional topology that enables energy exchange between two batteries with different voltage levels. One topology like that could be used to charge the auxiliary battery from the traction batteries. Although, according to the IEC 61851-1 standard it is mandatory that the traction batteries are maintained isolated from the vehicle chassis. Therefore, isolated DC-DC topologies are required to accomplish with this task. In [33] is proposed an interesting isolated topology that enables the charging of the auxiliary battery from the traction batteries, however, this topology requires a high number of controlled power semiconductors.

This paper proposes a simple, low-cost, and efficient solution that uses a reconfigurable on-board battery charger topology that, in addition to allow operation in Grid-to-Vehicle (G2V) and Vehicle-to-Grid (V2G) modes, also accomplish with the Traction-to-Auxiliary (T2A) battery charging operation mode without additional converters.

The proposed topology operates always with sinusoidal current and controlled reactive power in all range of operation (from minimum to full load), in both G2V and V2G modes. The sinusoidal current is important to keep the electrical power grid voltage with low distortion, particularly if there is a large number of EVs being charged simultaneously. The control of the reactive power is important to regulate the electrical power grid voltage, in order to keep it close to the nominal value. Considering that the line impedance of the electrical power grid is mostly inductive, if the battery chargers of the EVs, working collaboratively, operate with capacitive power factor, they contribute to increase the voltage in the Point of Common Coupling (PCC) of the power grid, otherwise, if they operate with inductive power factor, they contribute to decrease the voltage in the PCC.

II. Reconfigurable Battery Charger Operation Principle

Fig. 1 presents the electric diagram of the proposed reconfigurable battery charger. It is composed by three power stages. The first stage is a full-bridge AC-DC bidirectional

converter, the second stage is a reversible DC-DC converter, and the third stage is a full-bridge isolated DC-DC converter.

The power flow in each of the power converters depends on the operation modes. Fig. 2 presents the reconfigurable battery charger power flow for the different operation modes. Fig. 2 (a) presents the G2V and V2G modes of operation. In the G2V mode the active power (P) flows from the electrical power grid to the DC link, and from the DC link to the traction batteries. In the V2G mode the active power flows in the opposite way. In both these modes the battery charger can adjust the reactive power (Q), if requested. Fig. 2 (b) presents the T2A mode of operation, in which the energy flows from the traction batteries to the auxiliary battery.

The operation analyses of the reconfigurable battery charger for each of the three operation modes can be described as follows.

A. Grid-to-Vehicle (G2V) Mode

During this operation mode, sw_1 is closed and sw_2 is open (Fig. 1). The full-bridge AC-DC bidirectional power converter operates as an active rectifier with sinusoidal current absorption and controlled power factor, and the reversible DC-DC converter operates as a buck converter.

1) Full-Bridge AC-DC Bidirectional Converter Control

In order to accomplish with the maximum amplitude of the individual current harmonics specified by IEC 61000-3-2 standard, it is mandatory that the full-bridge AC-DC bidirectional power converter controller must be synchronized with the power grid fundamental voltage. Therefore, a single-phase Phase-Locked Loop (PLL) is the first algorithm implemented by the digital controller. This synchronizing algorithm is similar to the one implemented to three-phase systems [34], with some adaptations to single-phase systems [35]. In Fig. 3 is illustrated the block diagram of the single-phase α-β PLL algorithm. Also in this figure it can be seen that the feedback signals pll_α and pll_β are built up by the PLL algorithm based on the *sine* and *co-sine* of ωt, respectively (where ω is the angular frequency of the electrical power grid). These feedback signals have unity amplitude and pll_α leads 90º pll_β. When the PLL is synchronized, signals pll_α and pll_β are the direct and quadrature components of the power grid fundamental voltage. These signals are used as inputs to the subsequent digital control algorithms.

The reference current (i_S*) of the full-bridge AC-DC bidirectional converter is obtained by the sum of two components, one related with the active power and the other with the reactive power. The active power component (P*) is directly associated with the traction batteries charging current, and is achieved by a PI controller designed to keep the DC link voltage regulated.

The second component (Q*) defines the reactive power that the converter produces or absorbs and is established as an external input parameter. Both of active and reactive power components are multiplied, respectively, by the direct and quadrature components of the PLL (pll_α and pll_β) affected by a gain of $\sqrt{2}$. In Fig. 4 it can be seen the control block diagram of the full-bridge AC-DC bidirectional converter to generate the current reference (i_S*).

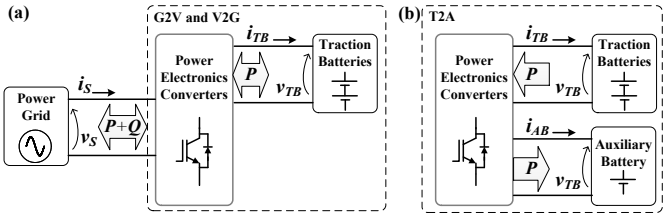

Fig. 2. Reconfigurable battery charger power flow: (a) During G2V and V2G operation modes; (b) During T2A operation mode.

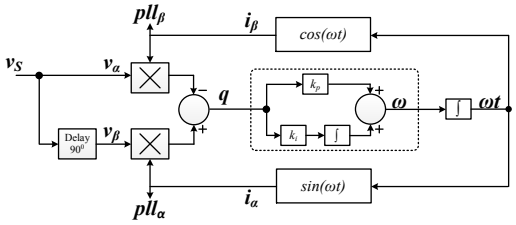

Fig. 3. Single-phase α-β PLL algorithm block diagram.

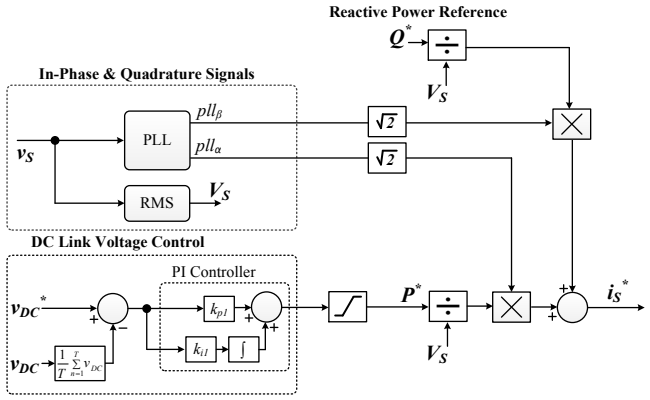

Fig. 4. Control block diagram of the full-bridge AC-DC bidirectional converter.

It is important to note that the maximum value of reactive power (Q) that the converter can produce is limited by the maximum admissible apparent power (S) of the full-bridge AC-DC bidirectional converter (the developed prototype was designed to be used in AC electrical power grids with nominal voltage of 230 V RMS and with maximum AC current of 16 A RMS, which results in an apparent power S = 3.6 kVA). Since the current at the AC side of the proposed battery charger is always kept sinusoidal, and considering that the power grid voltage is almost sinusoidal, the available reactive power can be approximated by:

$$Q = \sqrt{S^2 - P^2}, \tag{1}$$

therefore the maximum value of Q depends on the traction batteries charging stage, which defines the active power (P) being delivered to the traction batteries.

The power delivered to the traction batteries changes along the charging process, although during short time intervals it can be assumed constant. Therefore, considering that during an electrical grid cycle the batteries are charged with constant power, and since it is impossible to absorb constant power from an AC single-phase power grid operating with sinusoidal voltage and current, it is necessary to use an intermediary energy storage device. For that purpose, the battery charger uses a DC link capacitor, C_1 (Fig. 1). Since the energy stored in the capacitor along one grid cycle changes, its voltage also changes, with a periodicity of 2ω. In order to avoid that this

oscillation perturbs the current reference, it is used a sliding window average across the DC link voltage (v_{DC}) before the PI controller. Thereby, the PI controller only regulates the average DC link voltage (V_{DC}) in the capacitor, allowing the charge of the batteries with constant power, and absorbing sinusoidal current with constant amplitude from the power grid.

In order to synthesize the reference current (i_S*) calculated by the control algorithm, it is used a predictive current control. Aiming to implement the predictive current controller it is necessary to measure the power grid source voltage (v_S) and the source current (i_S). From Fig. 5 it can be established that:

$$v_S(t) = v_L(t) + v_R(t) + v_F(t)\,, \tag{2}$$

where the source voltage (v_S) is equal to the sum of the inductance voltage (v_L), the resistance voltage (v_R), and the voltage produced by the full-bridge AC-DC bidirectional converter (v_F). The resistance R represents the internal resistance of the coupling inductor, with inductance L_1, used in the AC side of the battery charger (Fig. 1).

The equation (2) can be written in order of the circuit parameters and of the source current (i_S), which is the variable to control, resulting in:

$$v_S(t) = L_1 \frac{di_S(t)}{dt} + R\, i_S(t) + v_F(t)\,. \tag{3}$$

Usually, the internal resistance of the coupling inductor presents small value and, therefore, its voltage drop can be neglected without introducing significant errors in the system model. So, (3) can be simplified as:

$$v_S(t) = L_1 \frac{di_S(t)}{dt} + v_F(t)\,. \tag{4}$$

The source current error ($i_{S\ error}$) is calculated as the difference between the reference current (i_S^*) and the produced source current (i_S):

$$i_{S\ error}(t) = i_S^*(t) - i_S(t)\,. \tag{5}$$

Substituting (5) in (4) and rearranging it in order to the voltage produced by the converter (v_F), it is obtained:

$$v_F(t) = -L_1 \frac{di_S^*(t)}{dt} + L_1 \frac{di_{S\ error}(t)}{dt} + v_S(t)\,. \tag{6}$$

Considering a high sampling frequency, the derivative of the reference (i_S^*) and error ($i_{S\ error}$) currents can be approximated by linear variations without introducing significant errors, as:

$$\frac{di(t)}{dt} \approx \frac{\Delta i}{\Delta t}\,. \tag{7}$$

Thus, (6) can be approximated by:

$$v_F(t) = -L_1 \frac{\Delta i_S^*}{\Delta t} + L_1 \frac{\Delta i_{S\ error}}{\Delta t} + v_S(t)\,. \tag{8}$$

Rewriting (8) in terms of discrete samples, where k is the actual sample and k-1 the previous sample, it is obtained:

$$v_F[k] = v_S[k] - \frac{L_1}{T}(i_S^*[k] - i_S^*[k-1] + i_{S\ error}[k] - i_{S\ error}[k-1])\,. \tag{9}$$

By replacing:

$$i_{S\ error}[k] = i_S^*[k] - i_S[k]\,, \tag{10}$$

in (9), it is obtained:

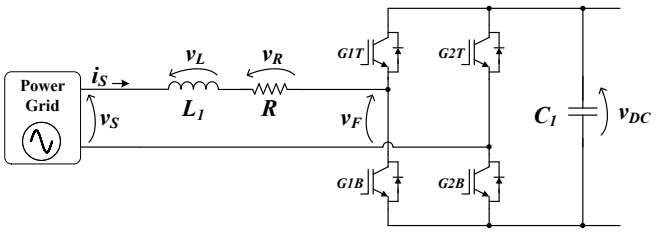

Fig. 5. Electric schematic of the full-bridge AC-DC bidirectional converter.

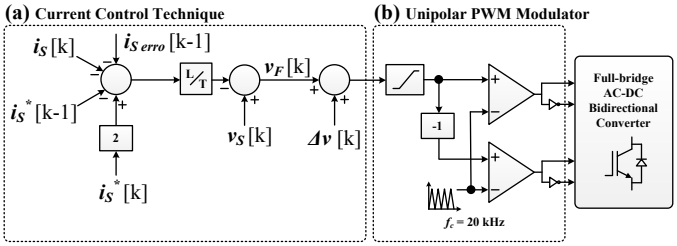

Fig. 6. Block diagram of the full-bridge AC-DC bidirectional converter digital controller: (a) Predictive current controller; (b) Unipolar PWM modulation technique.

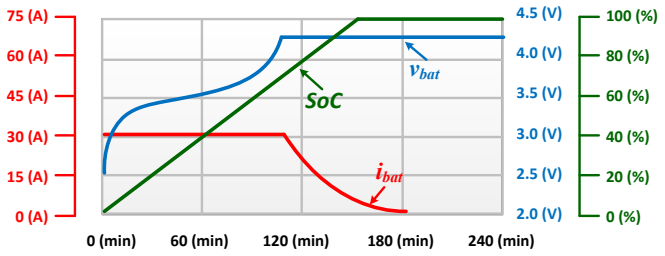

Fig. 7. Recommended two stages battery charging algorithm (Winston WB-LYP90AHA single-cell).

$$v_F[k] = v_S[k] - \frac{L_1}{T}(2i_S^*[k] - i_S^*[k-1] - i_S[k] - i_{S\ error}[k-1])\,. \tag{11}$$

The voltage (v_F [k]) is the reference voltage used to control the full-bridge AC-DC bidirectional converter. In order to obtain the gate pulse patterns to synthesize the reference voltage, calculated by the predictive current control algorithm, was used a unipolar sinusoidal pulse width modulator (PWM) with 20 kHz center aligned triangular carrier. To improve the output voltage of the full-bridge AC-DC bidirectional converter was implemented a digital dead-time compensation methodology. It consists in adding a voltage Δv (correspondent to the voltage error introduced by the dead-time) to the reference voltage [36]. The structure of the digital predictive current controller is shown in Fig. 6.

2) Reversible DC-DC Converter Control

The battery charger DC link voltage is always higher than the traction batteries voltage and for this reason during the G2V mode of operation the reversible DC-DC converter operates as buck converter.

Most of the EV batteries manufacturers recommend two charging stages: constant current followed by constant voltage. The first stage consists in charging the batteries with constant current until the voltage reaches the recommended maximum voltage, and in the second stage the voltage is maintained constant until the current consumed by the batteries falls to a residual value. Fig. 7 presents the

recommended charging stages for a single-cell battery *Winston WB-LYP90AHA* $LiFePO_4$ (90 Ah, 3.7 V) [37].

In order to accomplish with manufacturers recommendations, during the G2V mode the reversible DC-DC converter operates as buck converter controlled in both constant current and constant voltage stages, as shown in Fig. 8. In the constant current stage the reference current is compared with the actual current, and the current error feeds a PI controller that adjusts the output duty-cycle through a PWM modulator with a triangular carrier of 40 kHz. When the traction batteries voltage reaches the maximum value recommended by the manufacturer the control algorithm changes to the constant voltage stage. During this stage the output voltage of the reversible DC-DC converter is maintained constant with the help of a second PI controller.

To validate the topology and the control algorithms some simulations were carried out with PSIM 9.0 software. Fig. 9 presents the typical operating waveforms in the G2V mode during constant current charging stage, obtained with the simulation model. Fig. 9 (a) presents the voltage (v_S), the current (i_S), and the instantaneous power (p_S) in the electrical power grid, and the instantaneous power in the traction batteries (p_{TB}). Fig. 9 (b) presents the traction batteries voltage (v_{TB}) and current (i_{TB}) during the constant current charging stage. As it can be seen in this figure, the instantaneous power in the electrical power grid (p_S) oscillates between 0 and 7200 VA, but even though the power in the traction batteries (p_{TB}) is kept constant, equal to 3300 W. Taking into account that there is no reactive power ($Q = 0$), the battery charger operates with unitary power factor.

B. Vehicle-to-Grid (V2G) Mode

During this operation mode, sw_1 is closed and sw_2 is open (Fig. 1). The full-bridge AC-DC bidirectional power converter operates as an inverter with sinusoidal current injection and controlled power factor, and the reversible DC-DC converter operates as a boost converter.

1) Full-Bridge AC-DC Bidirectional Converter Control

Working as an inverter connected to the power grid, the full-bridge AC-DC bidirectional converter must be synchronized with the power grid fundamental voltage. The synchronization is obtained through a single-phase α-β PLL, as already explained in section *A,* subsection *1*, and shown in Fig. 3. The pll_α and pll_β synchronization signals are used as inputs to the subsequent digital control algorithms.

As occurs in the G2V mode, also in the V2G mode the current reference (i_S*) of the full-bridge AC-DC bidirectional converter is obtained by the sum of two components, one related with the active power and the other with the reactive power. These powers are established as external input parameters received from a digital port in order to enable a future Smart Grid integration. Taking into account these considerations, the control algorithm employed in the V2G mode is similar to the one used in the G2V mode (Fig. 4).

Aiming to synthesize the reference current previously calculated it was used a predictive current control, as described in section *A*, subsection *1*. The gate pulse patterns are obtained by synthesizing the reference voltage calculated by the predictive current control algorithm through a unipolar

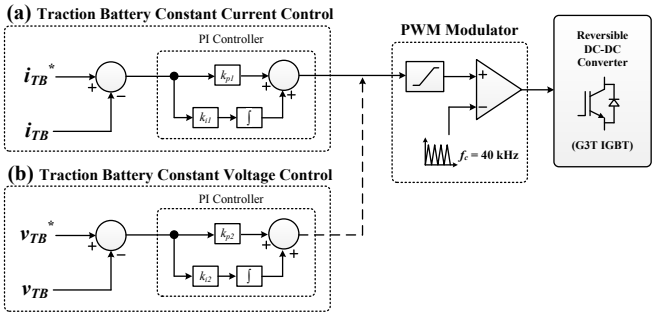

Fig. 8. Block diagram of the reversible DC-DC converter digital controller: (a) During constant current stage; (b) During constant voltage stage.

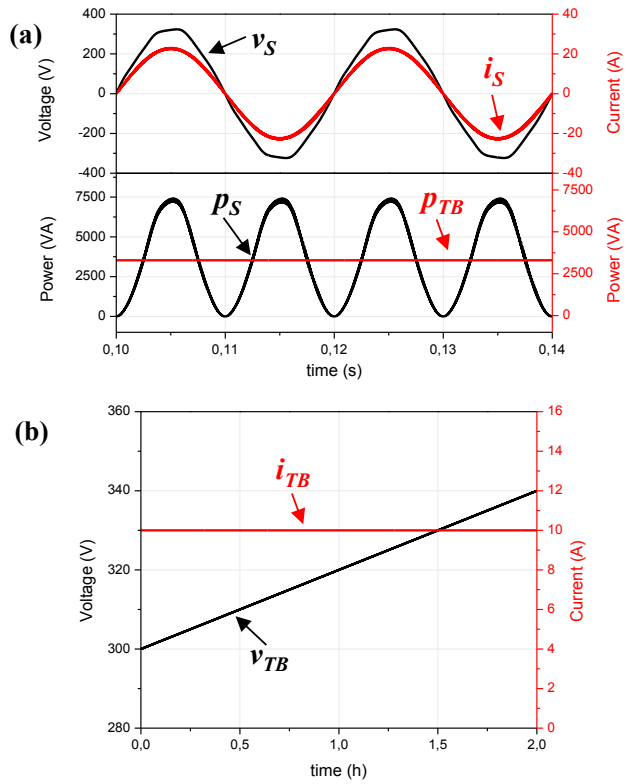

Fig. 9. Typical operating waveforms during the G2V mode and in the constant current charging stage: (a) Power grid voltage (v_S), current (i_S), instantaneous power (p_S), and instantaneous power (p_{TB}); (b) Traction batteries voltage (v_{TB}), current (i_{TB}).

sinusoidal pulse width modulator (PWM) with a 20 kHz center aligned triangular carrier. A dead-time compensation methodology is also used in this operation mode.

2) Reversible DC-DC Converter Control

The DC link voltage has to be greater than the peak value of the power grid voltage, in order that the full-bridge AC-DC bidirectional converter can deliver back to the power grid the energy stored in the traction batteries. Since the traction batteries voltage is below the required DC link voltage, the reversible DC-DC converter has to operate as a boost converter. Knowing that the traction batteries voltage does not suffer significant variation during short time periods, the regulation of the active power delivered back to the power grid is possible by the imposition of a constant current provided by the traction batteries. As the traction batteries voltage slightly decreases along the discharging process, to

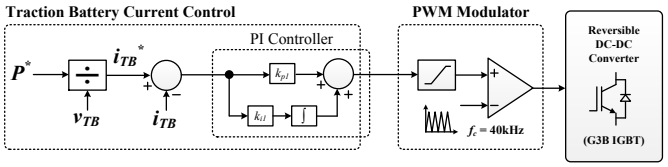

Fig. 10. Block diagram of the reversible DC-DC converter digital controller during the V2G mode.

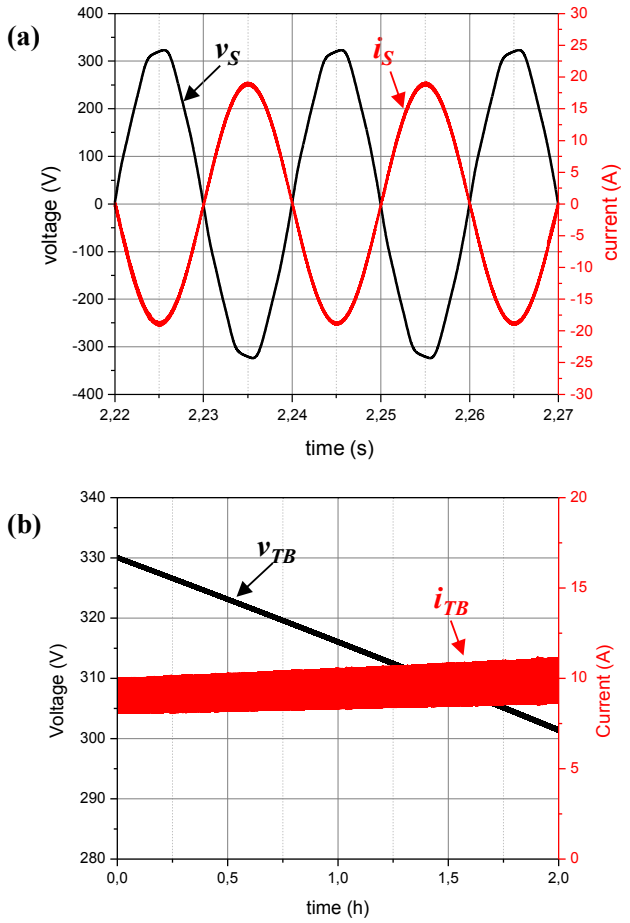

Fig. 11. Typical operating waveforms during the V2G mode: (a) Power grid voltage (v_S) and current (i_S); (b) Traction batteries voltage (v_{TB}) and current (i_{TB}).

maintain the active power constant it is necessary to increase the reference current for the traction batteries in the inverse proportion. Therefore, the traction batteries reference current (i_{TB}*) is calculated by dividing the reference power (P* - established as an external input parameter during V2G mode), by the traction batteries voltage (v_{TB}). The traction batteries current is obtained comparing a reference with the actual current, and then the resultant error feeds a PI controller that adjusts the output duty-cycle through a PWM modulator with a triangular carrier of 40 kHz, as shown in Fig. 10.

Fig. 11 presents the typical waveforms obtained with the simulation model during the V2G operation mode of the proposed reconfigurable battery charger, with constant active power (P = 3.6 kW) and without reactive power production (Q = 0) delivered to the power grid.

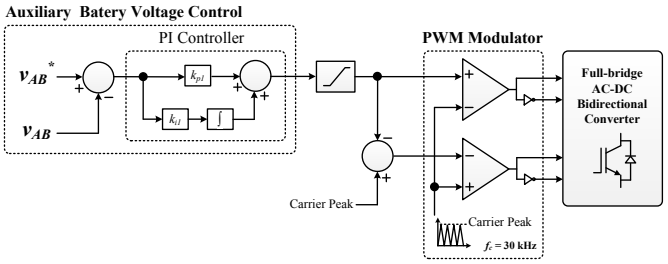

Fig. 12. Block diagram of the full-bridge isolated DC-DC converter digital controller during the T2A mode.

C. *Traction-to-Auxiliary (T2A) Mode*

During this operation mode, sw_1 is open and sw_2 is closed, reconfiguring the circuit in a full-bridge isolated DC-DC converter (the IGBTs from the full-bridge are used as the primary side of this converter) (Fig. 1). The reversible DC-DC converter is kept out of operation, with the IGBTs open.

However, the current flows from the traction batteries to the DC link through the reverse diode of the top IGBT (*G3T*). In this mode of operation the DC link voltage is almost equal to the traction batteries voltage. The high frequency transformer is used to attain the required galvanic isolation between the traction batteries and the auxiliary battery, and also to reduce the voltage level. The diodes D_1 and D_2 operate as full-wave rectifier, while L_3 and C_3 perform the output filter.

The auxiliary battery is not projected to work with high Depth-of-Discharge (DoD), and therefore, it is always charged with constant voltage. When the auxiliary battery voltage decreases more than a predefined value the converter starts the charging operation. When the current consumed by the auxiliary battery falls to less than a predefined residual value, the charging process stops.

In order to accomplish with the constant voltage charging process, the reference voltage is compared with the actual voltage, and the resultant error feeds a PI controller that adjusts the output duty-cycle through a PWM modulator, with a center aligned triangular carrier of 30 kHz. The switching frequency of the full-bridge IGBT is defined to this value as a compromise between the IGBTs switching losses and the size of the high frequency transformer and passive filter (components L_3 and C_3). The structure of the full-bridge isolated DC-DC converter digital controller is shown in Fig. 12. Therefore, the full-bridge isolated DC-DC converter operates with a power range from about 20 W to 500 W. In Fig. 13 are presented the typical operating waveforms during the T2A operation mode with an instantaneous power of 50 W. Fig. 13 (a) shows the voltage in the primary winding of the high frequency transformer (v_F) and the voltage in the auxiliary battery (v_{AB}), and Fig. 13 (b) shows again the voltage in the primary winding (v_F) and the current in the output filter inductor (i_{L3}).

III. Developed On-Board Reconfigurable Battery Charger

In the development of the on-board reconfigurable battery charger prototype the specification of the electronic components has taken into account the compromises between cost, size, and efficiency. The main specifications of the

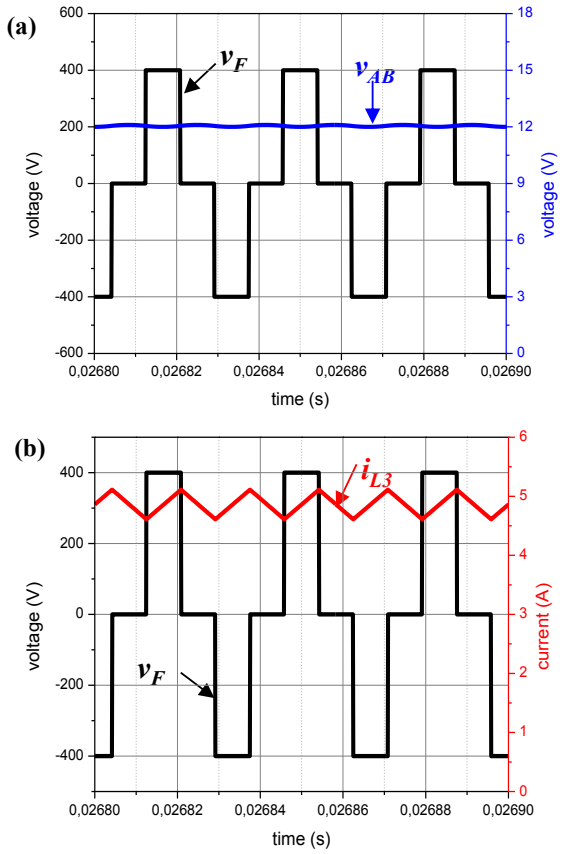

Fig. 13. Typical operating waveforms during the T2A mode: (a) Voltage in the primary winding of the high frequency transformer (v_F) and voltage in the auxiliary battery (v_{AB}); (b) Voltage in the primary winding (v_F) and current in the output filter inductor (i_{L3}).

reconfigurable battery charger prototype are given in TABLE I.

In the three-level full-bridge AC-DC bidirectional converter, the ripple of the AC current is dependent of the DC link voltage (v_{DC}), switching frequency, and coupling inductance value. It was considered as acceptable a ripple value (Δi_S) of 2% of the AC current peak (23 A). To achieve this goal, and considering that the circuit will operate with a DC link voltage (v_{DC}) with average value of 400 V and with a switching frequency of 20 kHz for each leg, which gives a resulting switching frequency (f_S) of 40 kHz, the coupling inductance has been selected to be 5 mH, in accordance with:

$$L_1 = \frac{v_{DC}}{4\,\Delta i_S\, f_s}\ . \tag{12}$$

As aforementioned, the power delivered to the battery is constant, and since it is impossible to absorb constant power from a single-phase power grid, it is necessary to use an intermediary energy storage device, which corresponds to the DC link capacitor, C_1 (Fig. 1). The sizing of this element is a key factor for the proper operation of the full-bridge AC-DC bidirectional converter. Therefore, considering that:

$$v_S(t) = \sqrt{2}\,V\,sen(\omega t)\,, \tag{13}$$

and that:

$$i_S(t) = \sqrt{2}\,I\,sen(\omega t + \phi)\,, \tag{14}$$

the instantaneous power is defined by:

TABLE I
DESIGN SPECIFICATIONS OF THE PROPOSED BATTERY CHARGER

Parameters	VALUE	UNIT
Input AC Voltage (RMS)	230 ± 10%	V
AC Input Frequency	50 ± 1%	Hz
Maximum Input AC Current (RMS)	16	A
Input AC Maximum Current Ripple	0.5	A
Maximum Input Power	3.6	kVA
Power Factor @ Full Load	0.99	
THD_i @ Full Load	< 3%	
Output DC Voltage Range	270 to 360	V
Output DC Voltage Ripple	0.04	V
Output DC Current Ripple	0.2	A
Maximum Output DC Current	10	A
Maximum Output Power	3.5	kW
Auxiliary Battery Voltage Ripple	0.24	V
Estimated G2V Efficiency	> 90%	
Estimated V2G Efficiency	> 90%	
Estimated T2A Efficiency	> 95%	
Prototype Dimensions	250 x 290 x 95	mm
Prototype Weight	4.9	kg

$$p(t) = \sqrt{2}\,V\,sen(\omega t)\,\sqrt{2}\,I\,sen(\omega t + \phi) = VI\cos(\phi) + 2VIcos(2\omega t + \phi) = \bar{p} + \tilde{p}\ ; \tag{15}$$

$$\bar{p} = VI\cos(\phi)\ ; \tag{16}$$

$$\tilde{p} = 2VIcos(2\omega t + \phi)\ ; \tag{17}$$

where, $\bar{p}$ is the average value of the instantaneous power, which corresponds to the energy per time unit transferred from the source to the load; and ($\tilde{p}$) is the oscillating value of the instantaneous power $p(t)$, which corresponds to the energy per time unit that is exchanged between the power source and the load. If the losses in the power converters are neglected, then the average value of the instantaneous power ($\bar{p}$) corresponds to the active power that continuously flows to charge the traction batteries. The oscillating value of the instantaneous power ($\tilde{p}$) is exchanged between the electrical power grid and the energy storage elements of the full-bridge bidirectional AC-DC converter (DC link capacitor, C_1, and coupling inductor, L_1, shown in Fig. 1). The energy exchanged with the DC link capacitor is considerable greater than the energy exchanged with the coupling inductor, and therefore the last one can be neglected in the design of the DC link capacitor without introducing significant error. The energy exchanged between the electrical power grid and the DC link capacitor causes a 2ω sinusoidal oscillation on the DC link voltage. Thus the DC link voltage can be expressed as a sum of two components:

$$v_{DC} = V_{DC} + \Delta v_{DC} \,, \tag{18}$$

where, V_{DC} is the average value of the DC link voltage capacitor, and is regulated by the control algorithm of the full-bridge AC-DC bidirectional converter (Fig. 4); and Δv_{DC} is the oscillating voltage amplitude that is dependent of the value of $\tilde{p}$ and of the capacitor energy storage capacity:

$$\frac{1}{2}\, C_1\, {v_{DC}}^2 = \int \tilde{p}\; dt \,. \tag{19}$$

Replacing (17) and (18) in (19), it is obtained:

$$C = \frac{2\, V_S\, I_S}{\omega\, \Delta v_{DC} V_{DC}} \,, \tag{20}$$

by which the DC link capacitor can be calculated.

Considering that a DC link voltage ripple of 2% of its maximum value (400 V) does not affect the operation of the battery charger, from (20) the DC link capacitance is calculated with a value of 3.6 mF. In the developed prototype this capacitance was obtained using four 820 µF / 450 V capacitors connected in parallel, which results in an equivalent value of 3.28 mF.

The traction batteries characteristics are significant to the design of the reversible DC-DC converter. During the G2V operation mode the batteries should be charged with a low ripple DC constant current and with a low ripple DC constant voltage to preserve the State-of-Health (SoH). On the other hand, during discharge (V2G operation mode), the batteries can support high ripple currents without deteriorating their characteristics. Consequently, the most demanding requirements to the design of the reversible DC-DC converter comes from the G2V mode of operation, during charging of the batteries.

In order to design the output filter of the reversible DC-DC converter, it was considered that the traction batteries has a minimum operating voltage of 270 V and an average Equivalent Series Resistance (ESR) of 0.2 Ω. The ESR depends of the battery technology, temperature, State-of-Charge (SoC) and SoH, and therefore it can change. Considering the ESR average value of the batteries and aiming a maximum battery ripple current of 0.2 A (2% of the maximum current of 10 A), the maximum battery voltage ripple (Δv_{TB}) becomes 0.04 V. Using this value it is possible to design the output filter (*L2* and *C2*) of the reversible DC-DC converter by means of:

$$L_2 C_2 = \frac{(v_{DC} - v_{TB})\, v_{TB}}{8\, {f_S}^2\, v_{DC}\, \Delta v_{TB}} \,, \tag{21}$$

which was derived from:

$$\Delta\, i_{L2} = \frac{(v_{DC} - v_{TB})\, \delta}{f_S\, L_2} = \frac{(v_{DC} - v_{TB})\, v_{TB}}{f_S\, L_2\, v_{DC}} \;; \tag{22}$$

$$\Delta\, i_{L2} = 8\, C_2\, f_s\, \Delta v_{TB} \;; \tag{23}$$

where δ is the duty-cycle.

Defining the value of L_2 equal to 300 µH, the value of C_2 must be greater than 571 µF to accomplish with the maximum current ripple specification. It is important to use low ESR capacitors to maintain the output voltage ripple near to the calculated value. In this application it selected a capacitor of 700 µF (a 680 µF aluminum electrolytic capacitor in parallel with a 20 µF polypropylene film capacitor).

TABLE II
KEY COMPONENTS OF THE PROPOSED BATTERY CHARGER

Device	PART / VALUE	Nº OF DEVICES
DSC	TMS320F28335	1
Transformer	n_1 / n_2 = 16.5	1
IGBT	FGA25N120ANTD	6
IGBT Drivers	HCPL3120	6
Diodes	IR 62CTQ030	2
Inductor L1	5 mH / 16 A	1
Capacitor C1	820 µF / 400 V	4
Inductor L2	300 µH / 15 A	1
Capacitor C2	700 µF / 400 V	1
Inductor L3	100 µH / 50 A	1
Capacitor C3	40 µF / 50 V	1
Current Sensor	LTSR 15-NP	2
Voltage Sensor	LV 25-P	4

During the T2A operation mode the auxiliary battery is charged through the full-bridge isolated DC-DC converter. Thus, this converter must also feed all the auxiliary electric circuits of the vehicle. In this prototype it is assumed that this power is less than 500 W. Therefore, the converter was designed to charge a 12 V auxiliary battery with a maximum power rate of 500 W.

As aforementioned, the converter that charges the auxiliary battery must have galvanic isolation from the traction batteries, and therefore a high frequency transformer with a turns-ratio of 66:4 was used. With this transformer, and considering a maximum DC link voltage of 400 V, the converter is able to control the output voltage in a range from 0 to 24 V.

Assuming a maximum battery ripple voltage of 0.24 V (2% of 12 V) it is possible to design the output filter (L_3 and C_3) of the full-bridge DC-DC isolated converter by means of (23). Defining the value of L_3 equal to 100 µH, the value of C_3 must be greater than 34 µF to accomplish with the maximum voltage ripple specification. In the developed prototype is used a capacitor of 40 µF.

The digital control system that implements the control algorithms of the proposed on-board reconfigurable battery charger is composed by several electronic circuits with analogue and digital signals, namely, sensors, signal conditioning circuits, voltage level shifters, and optocouplers. The key element of the controller is the Digital Signal Controller (DSC) TMS320F28335. It is an up-to-date device that operates at 150 MHz with native floating point support, and that includes the necessary peripherals to fulfill all the requirements of this application, namely, Analogue to Digital Converters (ADCs), PWMs, RAM, Flash Memory, and Enhanced Controller Area Network (eCAN). The design

Fig. 14. Developed reconfigurable battery charger prototype.

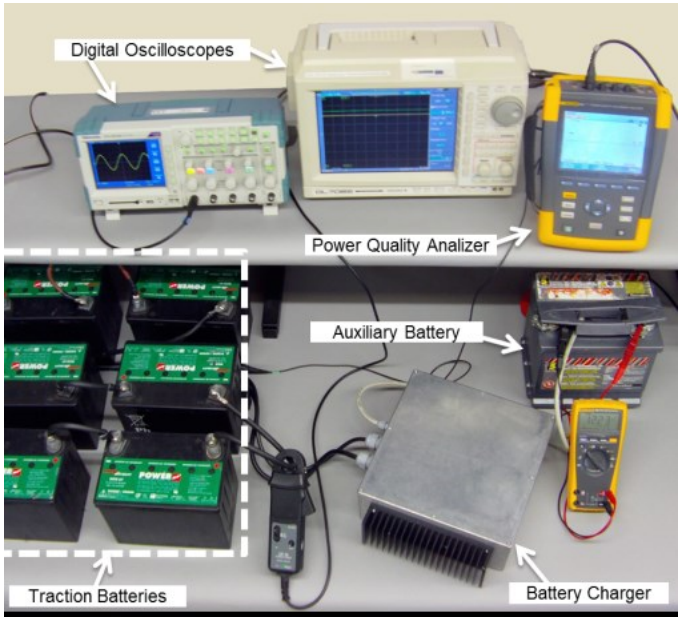

Fig. 15. Laboratory workbench.

specifications of the proposed reconfigurable battery charger are summarized in TABLE II.

In order to assess the operation of the reconfigurable battery charger under the different modes of operation it was developed and implemented a prototype considering the specifications summarized in Table I, and using the components of Table II. In Fig. 14 is presented the reconfigurable battery charger.

IV. Experimental Results

The developed prototype of the reconfigurable battery charger was submitted to a set of operation tests during the three operation modes (G2V, V2G and T2A). The reconfigurable battery charger is projected to work with any battery technology, and integrates a CAN-bus port to communicate with a standard Battery Management System

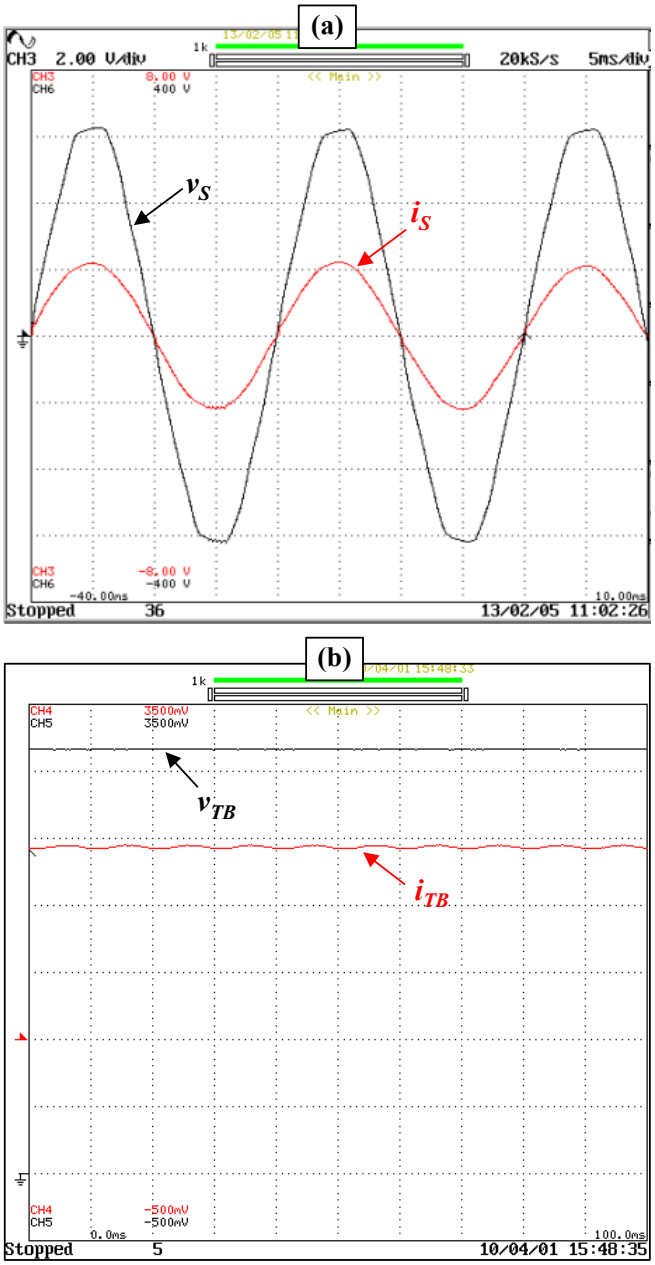

Fig. 16. Experimental results of the reconfigurable battery charger during the G2V mode: (a) Power grid voltage (v_S - 100 V/div) and current (i_S - 10 A/div); (b) Traction batteries voltage (v_{TB} - 100 V/div) and current (i_{TB} - 2 A/div).

(BMS). Both the traction batteries and the auxiliary battery used in the tests presented in this paper are based on the Absorbed Glass Mat (AGM) technology. In Fig. 15 is presented a photo of the laboratory workbench.

Due to other non-linear loads existing in the electrical installation, the waveform of the power grid voltage is distorted. Nevertheless, in all modes of operation the current consumed by the bidirectional power converter is sinusoidal, contributing to preserve the power quality of the electrical grid. Fig. 16 (a) shows the power grid voltage (v_S) and the absorbed current (i_S) during G2V mode of operation (with $P = 1.8$ kW and $Q = 0$), when the traction batteries are charged. It can be seen that the current is sinusoidal and in phase with the voltage (power factor is unitary). Fig. 16 (b)

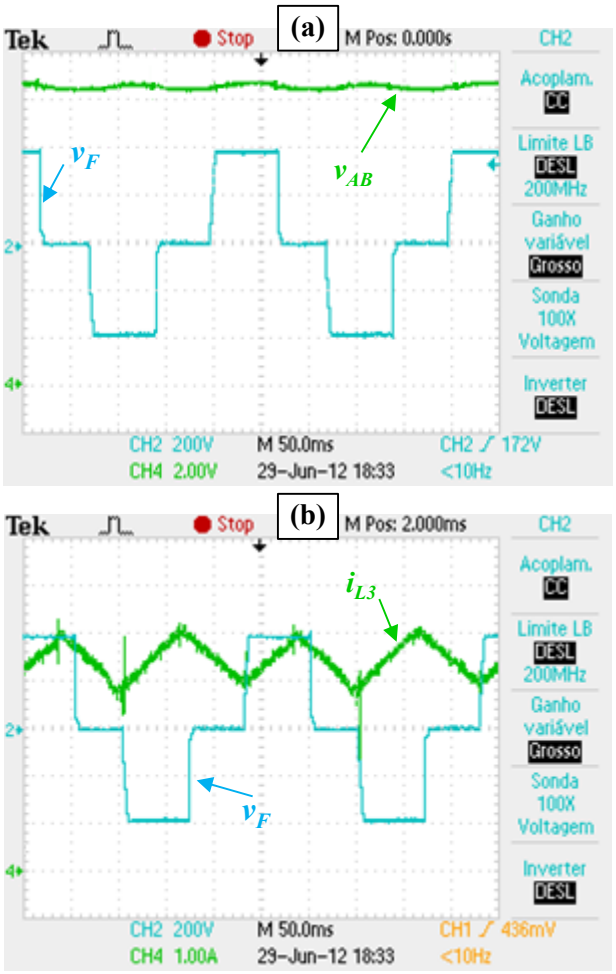

Fig. 17. Experimental results of the full-bridge isolated DC-DC converter during T2A mode of operation: (a) Voltage in the primary winding of the high frequency transformer (v_F - 200 V/div) and voltage in the auxiliary battery (v_{AB} - 2 V/div); (b) Voltage in the primary winding (v_F - 200 V/div) and current in the output filter inductance (i_{L3} - 1 A/div).

shows the obtained experimental results of the traction batteries voltage (v_{TB}) and absorbed current (i_{TB}) in the reversible DC-DC converter during G2V mode of operation. It can be seen that the battery charger accomplishes the objective of charging the batteries with constant current. It is important to notice that, although the voltage and current in the AC side of the battery charger are almost sinusoidal, resulting in oscillating power consumption, since the voltage and current provided to the traction batteries are constant, the batteries are charged with constant power. These results were registered with a Yokogawa DL708E digital oscilloscope.

The experimental results during the operation of the full-bridge isolated DC-DC converter are presented in Fig. 17. The voltage in the primary of the full-bridge isolated DC-DC converter, which correspond to the voltage in the primary winding of the high frequency transformer (v_F), and the auxiliary battery voltage (v_{AB}) are presented in Fig. 17 (a). The voltage in the primary winding (v_F) and the current in the inductance (i_{L3}) are shown in Fig. 17 (b). These results were registered with a Tektronix TPS-2024 digital oscilloscope.

In order to verify the accomplishement of the IEC 61000-3-2 standard regarding the specified maximum amplitude of the individual current harmonics, the reconfigurable battery charger was tested with a *FLUKE 435* Power Quality Analyzer.

Fig. 18 shows the experimental results of the reconfigurable battery charger during G2V operation mode with active power of 3.4 kW and without reactive power. Fig. 18 (a) shows the power grid voltage and the current waveforms and their True RMS values. Fig. 18 (b) presents the amplitude of the first 49 harmonics and the Total Harmonic Distortion (THD) of the current. Fig. 18 (c) presents the measured active, apparent and reactive powers and power factor. Fig. 19 shows the same experimental measurements of Fig. 18 during V2G operation mode with active power of 2.2 kW and reactive power of 1.5 kVAr (inductive reactive power).

V. Conclusion

In this paper is presented a reconfigurable battery charger for Electric Vehicles (EVs). This battery charger allows the interaction with the electrical power grid to charge the batteries (G2V - Grid-to-Vehicle mode) and to deliver part of the energy stored in the batteries back to the electrical power grid (V2G - Vehicle-to-Grid mode). In both operation modes the battery charger allows the regulation of the reactive power, and always works with sinusoidal current waveform in all range of operation (from minimum to full load), contributing to keep the electrical power grid voltage regulated and with low distortion. In order to operate with sinusoidal current, even with distorted electrical power grid voltage, it was used a grid synchronization algorithm, which consists in a single-phase α-β PLL. The requirements of low distortion and low ripple in the AC current demand an accurate current control algorithm. For that purpose, a fixed switching frequency predictive current control was implemented with successful results.

Furthermore to the G2V and V2G operation modes, the reconfigurable battery charger also allows the charging of the auxiliary battery with energy from the traction batteries (T2A – Traction-to-Auxiliary mode). This is a basic requirement for EVs, although usual battery chargers do not incorporate this functionality, and therefore a second additional converter is required. The presented topology proposes a solution that reuses the IGBTs of the full-bridge AC-DC bidirectional converter combined with a small high frequency transformer and two fast-recovery diodes, configuring a full-bridge isolated DC-DC converter. This reconfiguration avoids the use of an additional converter to charge the auxiliary battery, allowing the reduction of the size, weight and cost, when compared with traditional solutions. The use of the high frequency transformer guarantees the accomplishment of the IEC 61851-1 standard requirement of galvanic isolation between the traction batteries and the vehicle chassis.

The design and sizing of all the key components of the proposed reconfigurable battery charger was done using the mathematical models of the converters, and were validated through experimental tests in a prototype developed for that purpose. The main steps to design and size these key components are presented along the paper, as well as some illustrative experimental results. The experimental results obtained during the T2A operation mode of the reconfigurable

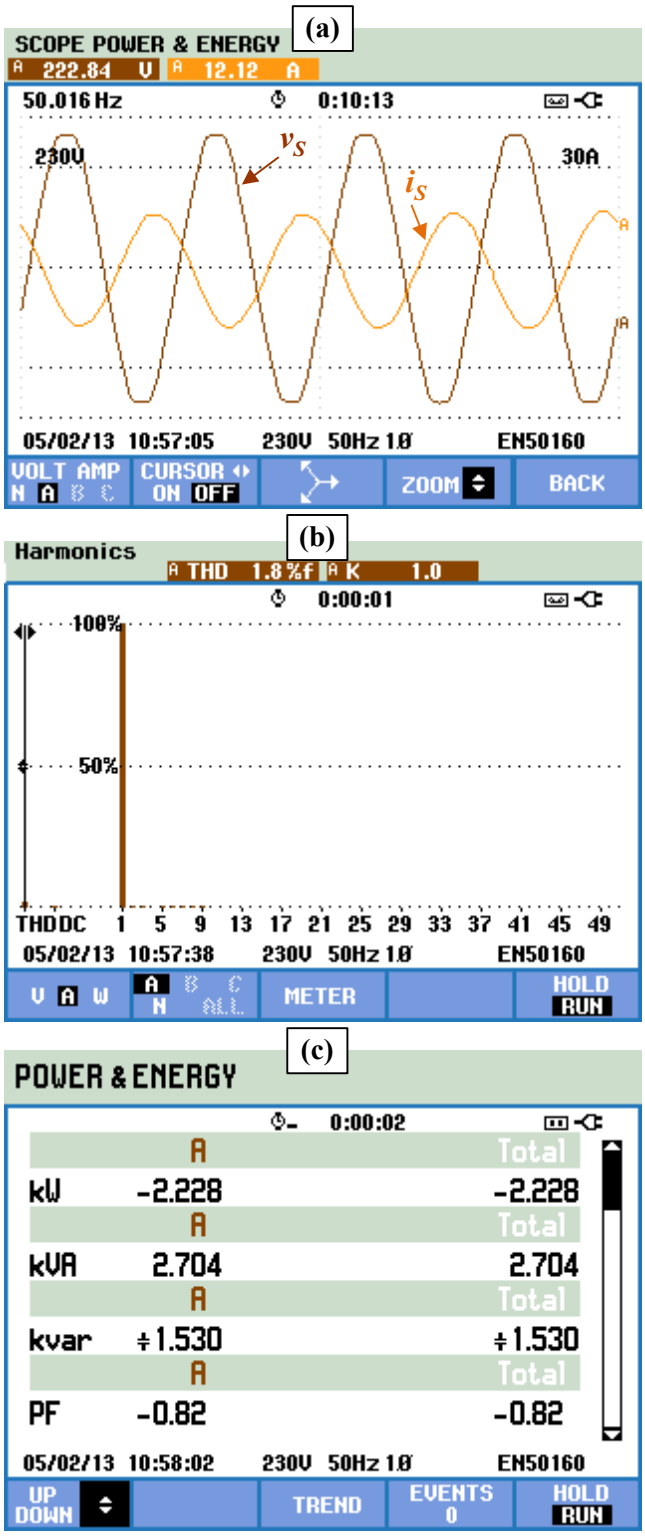

Fig. 18. Experimental results of the reconfigurable battery charger during V2G operation mode: (a) Power grid voltage (v_S) and current (i_S); (b) Current spectral analysis and THD; (c) Active, apparent and reactive powers and power factor.

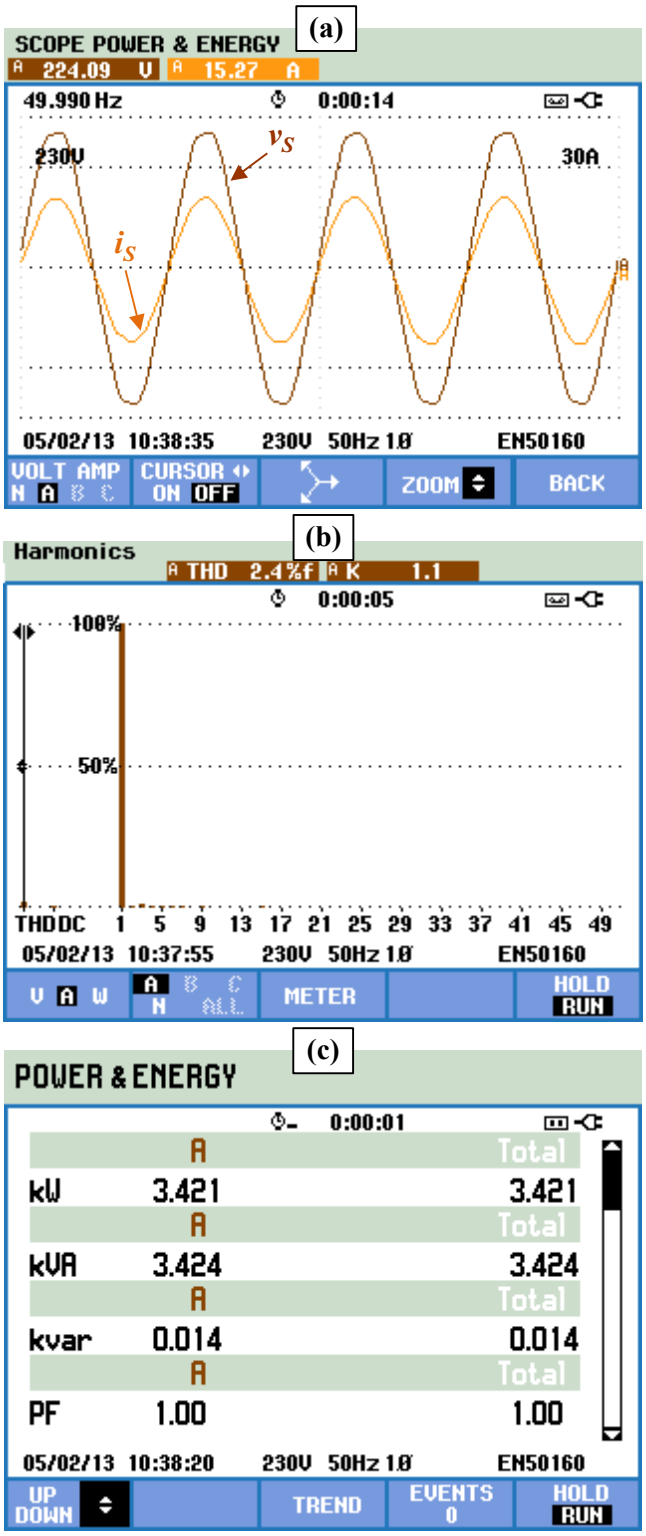

Fig. 19. Experimental results of the reconfigurable battery charger during G2V operation mode: (a) Power grid voltage (v_S) and current (i_S); (b) Current spectral analysis and THD; (c) Active, apparent and reactive powers and power factor.

battery charger are in accordance with the expected, validating the viability of the proposed topology. The accomplishment of the IEC 61000-3-2 standard, regarding the specified maximum amplitude of the individual current harmonics and the reactive power regulation, was verified with a *FLUKE 435* Power Quality Analyzer, during the G2V and the V2G operation modes.

In overall analysis it can be concluded that the proposed reconfigurable battery charger is very versatile, avoiding the need of additional converters to charge the auxiliary battery of

EVs, and fulfilling the main requirements for future integration in a smart grid.

ACKNOWLEDGMENT

This work is financed by FEDER Funds, through the Operational Programme for Competitiveness Factors – COMPETE, and by National Funds through FCT – Foundation for Science and Technology of Portugal, under the projects: FCOMP-01-0124-FEDER-022674, PTDC/EEA-EEL/104569/2008, AAC nº 36/SI/2009/13844, and MIT-PT/EDAM-SMS/0030/2008.

REFERENCES

[1] Farzad Rajaei Salmasi, "Control Strategies for Hybrid Electric Vehicles: Evolution, Classification, Comparison, and Future Trends," IEEE Trans. Veh. Technol., vol.56, no.5, pp.2393-2404, Sept. 2007.

[2] C.C.Chan, "The State of the Art of Electric, Hybrid, and Fuel Cell Vehicles," Proc. IEEE, vol.95, no.4, pp.704-718, Apr. 2007.

[3] Alireza Khaligh, Zhihao Li, "Battery, Ultracapacitor, Fuel Cell, and Hybrid Energy Storage Systems for Electric, Hybrid Electric, Fuel Cell, and Plug-In Hybrid Electric Vehicles: State of the Art," IEEE Trans. Veh. Technol., vol.59, no.6, pp.2806-2814, July 2010. .

[4] C. C. Chan, Alain Bouscayrol, Keyu Chen, "Electric, Hybrid, and Fuel-Cell Vehicles: Architectures and Modeling," IEEE Trans. Veh. Technol., vol.59, no.52, pp.589-598, Fev. 2010.

[5] Thomas A. Becker, Ikhlaq Sidhu, Burghardt Tenderich, "Electric Vehicles in the United States A New Model with Forecasts to 2030," University of California, Berkeley, Center for Entrepreneurship & Technology (CET), v.2.0, Aug. 2009. .

[6] J. Carlos Gómez, Medhat M. Morcos, "Impact of EV Battery Chargers on the Power Quality of Distribution Systems," IEEE Trans. Power Del., vol.18, no.3, pp. 975-981, July 2003.

[7] Kristien Clement-Nyns, Edwin Haesen, Johan Driesen, "The Impact of Charging Plug-In Hybrid Electric Vehicles on a Residential Distribution Grid," IEEE Trans. Power Syst., vol.25. no.1, pp.371-380, Feb. 2010.

[8] João A. Peças Lopes, Filipe Soares, Pedro M. Rocha Almeida, "Integration of Electric Vehicles in the Electric Power Systems," Proc. IEEE, vol.99, no.1, pp.168-183, Jan. 2011.

[9] Hal Turton, Filipe Moura, "Vehicle-to-grid systems for sustainable development: An integrated energy analysis," ELSEVIER Technological Forecasting and Social Change, vol.75, no.8, pp.1091-1108, Oct. 2008. .

[10] Mithat C. Kisacikoglu, Burak Ozpineci, Leon M. Tolbert, "Examination of a PHEV Bidirectional Charger System for V2G Reactive Power Compensation," IEEE APEC Applied Power Electronics Conference and Exposition, pp.458-465, Feb. 2010.

[11] Sekyung Han, Soohee Han, Kaoru Sezaki, "Development of an Optimal Vehicle-to-Grid Aggregator for Frequency Regulation," IEEE Trans. Smart Grid, vol.1, no.1, pp.65-72, June 2010.

[12] V.Monteiro, J.G.Pinto, B.Exposto, João C. Ferreira, C.Couto, João L. Afonso, "Assessment of a Battery Charger for Electric Vehicles with Reactive Power Control," IEEE IECON Industrial Electronics Society, Montréal-Canada, pp.5124-5129, Oct. 2012.

[13] W.Kempton, J.Tomic, "Vehicle-to-Grid Power Fundamentals: Calculating Capacity and net Revenue," Journal of Power Sources, vol.144, no.1, pp.268-279, Dec. 2004.

[14] PHEV Charging Strategies for Maximized Energy Saving.

[15] Zpryme Research & Consulting LLC, (July 2010). Smart Grid Insights: V2G, [Online]. Available: http://docs.zigbee.org/zigbee-docs/dcn/10-5873.pdf.

[16] Fariborz Musavi, Murray Edington, Wilson Eberle, William G. Dunford, "Evaluation and Efficiency Comparison of Front End AC-DC Plug-in Hybrid Charger Topologies," IEEE Trans. Smart Grid, vol.3, no.1, pp.413-421, Mar. 2012.

[17] Saeid Haghbin, Sonja Lundmark, Mats Alaküla, Ola Carlson, "Grid-Connected Integrated Battery Chargers in Vehicle Applications: Review and New Solution," IEEE Trans. Ind. Electron., vol.60, no.2, pp.459-473, Feb. 2013.

[18] Ernesto Inoa, Jin Wang, "PHEV Charging Strategies for Maximized Energy Saving," IEEE Trans. Veh. Technol., vol.60, no.7, pp.2978-2986, Sept. 2011.

[19] Alireza Khaligh, Serkan Dusmez, "Comprehensive Topological Analysis of Conductive and Inductive Charging Solutions for Plug-In Electric Vehicles," IEEE Trans. Veh. Technol., vol.61, no.8, pp.3475-3489, Oct. 2012.

[20] Michael G. Egan, Dara L. O'Sullivan, John G. Hayes, Michael J. Willers, Christopher P. Henze, "Power-Factor-Corrected Single-Stage Inductive Charger for Electric Vehicle Batteries," IEEE Trans. Ind. Electron., vol.54, no.2, pp.1217-1236, Apr. 2007.

[21] F.Musavi, M.Edington, W.Eberle, "Wireless Power Transfer: A Survey of EV Battery Charging Technologies," IEEE ECCE Energy Conversion Congress and Exposition, pp.1804-1810, Sept. 2012.

[22] Deepak S. Gautam, Fariborz Musavi, Murray Edington, Wilson Eberle, William G. Dunford, "An Automotive Onboard 3.3-kW Battery Charger for PHEV Application," IEEE Trans. Veh. Technol., vol.61, no.8, pp.3466-3474, Oct. 2012.

[23] IEEE Trial-Use Standard Definitions for the Measurement of Electric Power Quantities Under Sinusoidal, Nonsinusoidal, Balanced, or Unbalanced Conditions, IEEE Std 1459-2000, Jan. 2000.

[24] K.Kim, S.Park, S.Lee, T.Lee, C.Won, "Battery charging system for PHEV and EV using single phase AC/DC PWM buck converter," IEEE VPPC Vehicle Power and Propulsion Conference, pp.1-6, Sept. 2010.

[25] Majid Pahlevaninezhad, Pritam Das, Josef Drobnik, Praveen K. Jain, A.Bakhshai, "A New Control Approach Based on the Differential Flatness Theory for an AC/DC Converter Used in Electric Vehicles," IEEE Trans. Power Electron., vol.27, no.4, pp.2085-2103, Apr. 2012.

[26] Laszlo Huber, Yungtaek Jang, Milan Jovanovic, "Performance Evaluation of Bridgeless PFC Boost Rectifier," IEEE Trans. Power Electron., vol.23, no.3, pp.1381-1390, May 2008.

[27] Rebiha Metidji, Brahim Metidji, Boubkeur Mendil, "Design and Implementation of a Unity Power Factor Fuzzy Battery Charger using an Ultrasparse Matrix Rectifier," IEEE Trans. Power Electron., vol.28, no.5, pp.2269-2276, May 2013.

[28] D.Erb, O.Onar, A.Khaligh, "Bi-Directional Charging Topologies for Plug-in Hybrid Electric Vehicles," IEEE APEC Applied Power Electronics Conference and Exposition, pp.2066-2072, Feb. 2010.

[29] Vítor Monteiro, Henrique Gonçalves, João C. Ferreira, João L. Afonso, "Batteries Charging Systems for Electric and Plug-In Hybrid Electric Vehicles," in New Advances in Vehicular Technology and Automotive Engineering, 1st ed., J.P.Carmo and J.E.Ribeiro, Ed. InTech, pp.149-168, 2012.

[30] Omer C. Onar, Jonathan Kobayashi, Dylon C. Erb, Alireza Khaligh, "A Bidirectional High-Power-Quality Grid Interface With a Novel Bidirectional Noninverted Buck–Boost Converter for PHEVs," IEEE Trans. Veh. Technol., vol.61, no.5, pp.2018-2032, June 2012.

[31] X.Zhou, G.Wang, S.Lukic, S.Bhattacharya, A.Huang, "Multi-Function Bi-directional Battery Charger for Plug-in Hybrid Electric Vehicle Application," IEEE ECCE Energy Conversion Congress and Exposition, pp.3930-3936, Sept. 2009.

[32] Young-Joo Lee, Alireza Khaligh, Ali Emadi, "Advanced Integrated Bidirectional AC/DC and DC/DC Converter for Plug-In Hybrid Electric Vehicles," IEEE Trans. Veh. Technol., vol.58, no.8, pp.3970-3970, Oct. 2009.

[33] Sung Young Kim, Hong-Seok Song, Kwanghee Nam, "Idling Port Isolation Control of Three-Port Bidirectional Converter for EVs," IEEE Trans. Power Electron., vol.27, no.5, pp.2495-2506, May 2012.

[34] Luís Guilherme Barbosa Rolim, Diogo Rodrigues Costa, Maurício Aredes, "Analysis and Software Implementation of a Robust Synchronizing PLL Circuit Based on the pq Theory," IEEE Trans. Ind. Electron., vol.53, no.6, pp.1919-1926, Dec. 2006. .

[35] H.Carneiro, L.F.C.Monteiro, João L. Afonso, "Comparisons between Synchronizing Circuits to Control Algorithms for Single-Phase Active Converters," IEEE IECON Industrial Electronics Conference, pp.3229-3234, Nov. 2009.

[36] Alfredo R. Munoz, Thomas A. Lipo, "On-Line Dead-Time Compensation Technique for Open-Loop PWM-VSI Drives," IEEE Trans. Power Electron., vol.14, no.4, pp.683-689, July 1999.

[37] Winston Battery, "Lithium Battery datasheet WB-LYP90AHA," Charge and Discharge Chart, Jan. 2007.

J. G. Pinto (S'06) was born in Guimarães, Portugal, in 1977. He received the degree in Industrial Electronics Engineering and the M.Sc. degree in Industrial Electronics from the University of Minho, Portugal, in 2001 and 2004, respectively. From 2002 to 2006 worked as invited Assistant Lecturer at the Electrical Department of the Polytechnic Institute of Bragança, Portugal. From 2006 to 2012 he worked as a researcher at the Group of Energy and Power Electronics (GEPE) of the Centro Algoritmi, at the University of Minho. He received the PhD degree in Electronics and Computer Engineering from the University of Minho, in 2012. Since 2013 he works as invited Assistant Professor at the Industrial Electronics Department of the University of Minho. His research interests are related with Power Electronics, Power Quality and Digital Control of Power Converters.

Vítor Monteiro (S'10) was born in Guimarães, Portugal, on May 1984. He received the M.Sc. in Industrial Electronics and Computers Engineering, from the School of Engineering of the University of Minho, in 2012. Since 2008 he is a member of the Group of Energy and Power Electronics (GEPE) of the Centro Algoritmi, at the University of Minho. Currently he is a PhD student supported by the doctoral scholarship SFRH/BD/80155/2011 granted by the Portuguese FCT agency, and a collaborator of the Centro Algoritmi of the University of Minho. His research interests are related with Power Electronics Converters, Digital Control Techniques, Smart Grids, and Electric Vehicles.

Henrique Gonçalves (S'02-M'10) was born in Valongo, Portugal, in 1975. He is Assistant Researcher at the Centro Algoritmi of the University of Minho since 2009. He was Assistant Lecturer at the Department of Electrical Engineering of the Polytechnic Institute of Bragança between 1999 and 2006. He has completed his PhD in Electrical and Computer Engineering in the Faculty of Engineering of University of Porto in 2008. He has finished his Bachelor of Electrical Engineering at the Instituto Superior de Engenharia do Porto in 1996, and also a degree and M.Sc. in Electrical and Computer Engineering at the Faculty of Engineering, University of Porto, in 1998 and 2001 respectively. His research work relates to the development of power electronics for electric vehicles and renewable energy power generation.

João Luiz Afonso (M'00) was born in Rio de Janeiro, Brazil, in 1963. He is Associate Professor at the Department of Industrial Electronics of the University of Minho, Portugal, where he works since 1993. He received the degree in Electrical Engineering and the M.Sc. degree in Electrical Engineering from the Federal University of Rio de Janeiro, Brazil, in 1986 and 1991, respectively. In 2000 he obtained his PhD in Industrial Electronics from the University of Minho, Portugal. He lectures the subjects of Electrical Machines, Complements of Power Electronics, Electrical Power Quality, Active Power Filters, and Renewable Energy. His researching activities are related with the development of Active Power Filters, Power Quality Analyzers, Power Electronics for Renewable Energy Sources and Electric Vehicles, and with studies of Power Quality and Energy Efficiency.